Effectiveness of projectile screening in single and multiple ionization of Ne by B^{2+}

W. Wolff,[1] H. Luna,[1] A. C. F. Santos,[1] E. C. Montenegro,[1] R. D. DuBois,[2] C. C. Montanari,[3] and J. E. Miraglia[3]
[1]*Instituto de Física, Universidade Federal do Rio de Janeiro, Caixa Postal 68528, Rio de Janeiro, 21945-970 RJ, Brazil*
[2]*Department of Physics, Missouri University of Science and Technology, Rolla, Missouri 65409, USA*
[3]*Instituto de Astronomia y Fisica del Espacio, Casilla de Correo 67, Sucursal 28, C1428EGA, Buenos Aires, Argentina*
(Received 27 June 2011; published 10 October 2011)

Pure multiple ionization cross sections of Ne by B^{2+} projectiles have been measured in the energy range of 0.75 to 4.0 MeV and calculated using the continuum distorted wave-eikonal initial state approximation. The experiment and calculations show that the ionization cross sections by B^{2+}, principally for the production of highly charged recoils, is strongly enhanced when compared to the bare projectile with the same charge state, He^{2+}, at the same velocities.

DOI: 10.1103/PhysRevA.84.042704 PACS number(s): 34.50.Fa

I. INTRODUCTION

Ionization of multielectron atoms by dressed ions is a key process in several areas of basic and applied physics. To date, this process still has a limited understanding concerning several important dynamical features due not only to the conceptual complexity of treating many-electron transitions, but also due to the small number of absolute measurements recording the recoil ion charge states available in the literature, which restricts more stringent tests for theoretical calculations.

Collisions involving multielectron targets and swift ions can lead to transitions of one or more target electrons to various final states. In collisions with heavy ions, several collision channels are not only important but also strongly coupled among themselves. The independent electron approximation has been widely used as a useful starting point for the analysis of both inclusive (when the collision channels leading to different charge states of the projectile and the target are not separated in the measurements) and exclusive (when the collision channels leading to different charge states of the projectile and the target are separately measured) cross sections of multielectron systems [1–4] in connection with the energy deposition model [5], the classical trajectory Monte Carlo calculations [6–8], or quantal calculations [9,10].

In the case of exclusive studies of multiple ionization by multiple-charged projectiles, Kirchner *et al.* [11] used the semiclassical approximation with a coupled mean-field description of initial projectile and target electrons as an approximate time-dependent Hartree-Fock method to calculate the total cross sections for single-electron transfer, pure ionization, and single-projectile electron loss and compare with experiments for C^{3+} projectiles on Ne. This was the first fully quantum-mechanical comprehensive study in this subject. More recently, other calculations for few-electron ions have been performed to describe multiple ionization. The continuum distorted wave-eikonal initial state (CDW-EIS) approximation has been used by Galassi *et al.* [9] and Montanari *et al.* [10] to obtain multiple ionization cross sections by single-charged H^+ and He^+ ions in noble gases, in the intermediate- to high-velocity regime, yielding good agreement with the experiment. A different model based on the transport equation was used by Archubi *et al.* [12] to calculate multiple ionization of noble gases by swift H^+. This model differs from the independent-particle approximation in that it leads to a Poisson distribution for multiple ionization and gives results that are similar to the CDW-EIS model.

In addition to the difficulty of treating the collisional processes for a broader range of projectile energies and charge states, one further ingredient hiding the direct comparison between theoretical models and the measurements is the indirect relationship between the collisional process and the measured charge state of the target ion. Indeed, inner or deeper valence shell ionization followed by postcollisional electron emission, like Auger, Coster-Kronig, or shake-off processes, can generate a vacancy cascade and highly charged target ions are produced after the collisional process. Only recently, after the exclusive measurement of multiple ionization of Ne by fast protons [13], the dynamic signatures of these time-delayed mechanisms were clearly identified and a good description of multiple ionization was obtained by combining the independent electron approximation with branching ratios for multiple ionization obtained from photoionization measurements [14–19]. This approach has been successfully used in the last years to describe multiple ionization in the intermediate- to high-velocity regime for several multielectron atoms [9,10,12,13,20,21,29,30].

On the experimental side, several experiments have been carried out using He as a target but, for heavier targets, exclusive coincidence measurements of absolute cross sections are not so numerous and they are mainly focused to explore some specific regime and features of the collision dynamics of multielectron transitions. As Ne has been considered a benchmark target for multiple ionization studies, we limit our review to measurements for which this target is included.

Absolute cross section measurements for ionization of Ne by heavy projectiles were carried out by Cocke [5] using Cl^{q+} beams ($q = 6$–13) at $\sim$1.0 MeV/amu to produce recoil ions with high charge states (up to $q = 8$ on Ne). That work was followed by others which, in addition to the recoil ions' charge states, projectile charge states were concomitantly measured to determine either pure multiple ionization cross sections, or cross sections for multiple ionization associated with electron capture or electron loss. Most of these experiments were designed to study the production of highly charged recoil ions by highly charged projectiles [7,8,22–24] and only a few reported target multiple ionization by dressed projectiles with low-charge states ($q \leqslant 3$) [11,25–27], or molecular ions as projectiles [29,30].

In the course of penetration of heavy ions in matter, ionization by low-charge, dressed-ions is the dominant channel at the region of the trajectory where the ion reaches the distal part of the Bragg peak, which is the position of the trajectory where ionization is maximum. This is an important region of the projectile trajectory for many applications, ranging from technology to medicine and tumor therapy. The understanding of the collision dynamics in this region is essential to obtain the local damage. From the point of view of collision dynamics this region corresponds to the intermediate- to low-velocity regime. In this regime electron capture is coupled with ionization and collisions at small impact parameters are important. Within this scenario, the effective charge of the projectile along the ionization process can be larger than the projectile charge. How much larger is an important question, which depends both on the collision dynamics and on the electronic configuration of the projectile.

In this paper we report exclusive, absolute cross sections for multiple ionization of Ne by B^{2+} projectiles in the 0.69–370 keV/amu energy range. The projectile charge state is the same before and after the collisions. B^{2+} has a $1s^2 2s$ electronic configuration with the $2s$ radius around 0.87 Å, approximately five times the $1s$ B^{2+} radius and 1.7 times the Ne $2p$ radius [28]. The large $2s$ radius of B^{2+} compared with the Ne atomic radius makes this projectile well suited to study the partial screening of the projectile because it changes significantly along the ionization trajectory. The experimental results are compared with continuum distorted wave-eikonal initial state (CDW-EIS) including the postcollisional contribution and an inhomogeneous screening, $Z_{\mathrm{eff}}(p)$, of the projectile, dependent on the momentum transfer p.

The paper is organized as follows. In Sec. II, the experimental setup and the procedures to obtain the absolute cross sections are described. In Sec. III, the methodology to obtain the Ne multiple ionization cross section within the CDW-EIS approximation is presented. The discussion of the theoretical and experimental results and the comparison between them are drawn in Sec. IV. Finally, Sec. V presents a summary of the main conclusions of this work.

II. EXPERIMENT

The present experiment was carried out at the Tandem Pelletron accelerator facility of the Physics Institute at the Rio de Janeiro Federal University. A negative ion beam of boron was created from a mixture of metallic boron and silver powder (about 1:1 by volume) and extracted from the SNICS-II ion source at 7 kV. The B- ions were preaccelerated, velocity analyzed by a Wien filter, delivered to the entrance of the accelerator and then accelerated toward the terminal, where they passed through a N_2 stripper gas cell located in the middle of the accelerator. The positively charged B^{2+} ions produced, experienced a second acceleration, reaching the final beam energy at the high end of the accelerator. The B^{2+} ions at energies ranging from 0.75 to 4.0 MeV were selected by a switching magnet (SM) and directed to the ion-atom collision beam line, which was kept at a high vacuum of 3×10^{-8} Torr, located at a 15° angle relative to the exit of the SM. This beam line holds three chambers in sequence: a gas cell chamber, a gas jet interaction chamber, and a projectile detection chamber. With this setup, it is possible to measure independent, absolute, exclusive cross sections for the production of recoil ions through the electron capture, electron loss, or direct ionization channels, as described in detail below.

The B^{2+} ions were first collimated by a pair of four jaw slit assemblies separated from each other by approximately 2.0 m. The first collimator set was placed immediately after the entrance of the beam line. Using both sets of adjustable slits, the incident ions counting rate was reduced to approximately 1–3 kHz, the incoming ion beam size was defined to less than 2.0 mm and the beam angular divergence was limited in order to pass the beam through the gas cell chamber with negligible scattering.

A horizontal parallel plate electrostatic deflector (0.3 m in length), located immediately prior to the gas cell chamber, was used to direct the beam through the 2.5 mm entrance and the 3.0 mm exit aperture of the differentially pumped gas cell, and to clean the main beam from neutral- and charge-state impurities generated from the residual gases and slit contamination. The length of the cylindrical gas cell was 12.0 cm, defining a total collision path length of 12.6 cm, where the additional length accounts for gas leakage through the entrance and exit apertures. After the chamber, a vertical electrostatic plate deflector, 0.6 m long, was used to discriminate the emerging projectiles charge states after the collision with the target gas cell.

The interaction jet chamber was located 1.5 m downstream from the gas cell chamber. In this collision chamber, the time of flight mass spectrometer (TOF), coupled to a linear motion manipulator, the effusive gas jet assembly, attached to an XYZ manipulator, and a full-range pressure gauge were installed. A vertical beam deflector located prior to the interaction chamber was used to carefully center the incoming beam vertically with respect to the spectrometer extracting electrodes as well as to the position sensitive detector installed at the end of the beam line. The transverse position (with respect to the beam) of the spectrometer and the gas jet were adjusted with the linear motion and XYZ manipulators. The spectrometer extraction grids and gas jet assembly were placed at the center of the interaction chamber.

The separation of the different charge states of the beam emerging from the interaction region was made by a second electrostatic analyzer, consisting of 60-cm parallel electrodes, 1.5 cm apart, placed just after the exit aperture of the interaction jet chamber. After colliding with the Ne target, the projectiles were charge-state analyzed by this deflector and finally directed to the projectile detection chamber, 2 m downstream from the center of the interaction jet chamber. In this projectile detection chamber, a position-sensitive resistive anode detector, a surface barrier detector and a dynode-channeltron detector are housed. On the position-sensitive detector, up to four different charge states of the projectile could be collected simultaneously, while the surface barrier detector could detect only one charge state at a time.

The absolute cross sections of the total electron capture and electron loss channels were determined using the standard growth-rate method, described in detail by Tawara and Russek [31]. The experimental procedures and analysis performed in this work were the same used and described in detail in Ref. [32]. Briefly, the incident B^{2+} projectiles enter the differentially pumped gas cell chamber where the Ne gas, with

increasing target thicknesses, varying from 0.01 to 0.30 mTorr, was supplied through an all metal ultrafine leak valve. The pressure was measured by an absolute capacitive manometer directly connected to the cell chamber. The spatial separation of the different projectile charge states emerging from the cell on the position-sensitive detector was done by a vertical electrostatic plate deflector, as mentioned above. In order to connect the data for the different detectors used in this work, the experiment was also performed using a surface barrier detector, which can be moved to collect the projectile states at two different positions, not simultaneously. The consistency of the data from position-sensitive detector to surface barrier detector was checked through the ratio between electron capture and electron loss cross sections measured on both detectors. The cross sections obtained for the capture channel were compared directly with the previous work with very good agreement. For consistency, the absolute total capture cross section was measured for each collision energy under the same experimental conditions. This was used to normalize the subsequent measurements of electron capture, transfer ionization, and pure ionization cross sections.

The multiply ionized recoil ions and emitted electrons produced by the incident B^{2+} beam under single-collision conditions were collected by a time of flight spectrometer divided in two opposite regions: the recoil ion and the electron sides. The extraction field was applied in the interaction region by pair of electrodes, separated from each other by 1.0 cm. The electrodes were constructed from 89% transmission grids, and biased with symmetric voltages of ± 350 V. On the recoil ion side, the recoil ions were focused by a lens, and then passed through a 190-mm field-free time of flight tube with grids at the entrance and the exit. They were detected by a 24-mm diameter chevron microchannel plate and collected by a time readout anode. On the electron side, the ejected electrons were directed by a focusing and Einzel-lens assembly toward a 12 mm diameter channeltron. Ion trajectory simulations showed that H^+ ions ejected at any arbitrary angle to the extraction field were detected if their energy was lower than 10 eV and likewise electron trajectory simulations showed full acceptance of electrons with energies up to 40 eV, irrespective of the direction of emission. Coincidences between the recoil ion and either the electron signals or the surface barrier projectile detector are carried out using standard NIM fast electronics.

Two coincidence spectra were recorded for the pure ionization channel: one recoil ion B^{2+} projectile spectrum and one electron-recoil ion coincidence spectrum. For the capture channel, also two coincidence spectra were recorded, but, in this case, one recoil ion B^+ projectile spectrum and again one electron-recoil ion coincidence spectrum. These coincidence measurements, together with those for total electron capture, allowed us to obtain absolute cross sections for pure multiple ionization of Ne independently of any previous measurements.

III. THEORY

Within the independent particle model, the probability of multiple ionization can be related to the single ionization probability, $p_{\rm nlm}(b)$, of the electronic initial state nl as a function of the impact parameter $\vec{b} = \{b,\ \varphi_b\}$, via the multinomial distribution (see Eqs. (1) and (2) of Ref. [10]).

In this contribution all the initial states of the Ne electrons were considered, $nlm = 2p_0,\ 2p_{\pm 1},\ 2s$, and $1s$. The probabilities were computed with the help of the two-dimensional Fourier transform of the T-matrix elements

$$p_{\rm nlm}(E,\Omega,\vec{b}) = \int \frac{d\vec{\eta}}{2\pi} \exp(i\vec{\eta}\cdot\vec{b}) T_{\rm nlm}(E,\Omega,\vec{\eta}), \quad (1)$$

where $\vec{\eta} = \{\eta,\varphi_\eta\}$is the transversal momentum transfer and $E(\Omega)$ is the energy (angle) of the ejected electron. It is convenient to expand $T_{\rm nlm}$ as follows:

$$T_{\rm nlm}(E,\Omega,\vec{\eta}) = \sum_{\mu=-M}^{M} i^\mu \frac{\exp(i\mu\,\varphi_\eta)}{\sqrt{2\pi}} T_{{\rm nlm}\mu}(E,\Omega,\eta) \quad (2)$$

to produce

$$a_{\rm nlm}(E,\Omega,\vec{b}) = \sum_{\mu=-M}^{M} i^\mu \frac{\exp(i\mu\,\varphi_b)}{\sqrt{2\pi}} a_{{\rm nlm}\mu}(E,\Omega,b), \quad (3)$$

with

$$a_{{\rm nlm}\mu}(E,\Omega,b) = i^{-\mu} \int_0^\infty \eta\, d\eta\, J_\mu(b\eta) T_{{\rm nlm}\mu}(E,\Omega,\eta), \quad (4)$$

and with $J_m(b\eta)$ being the cylindrical Bessel function. The total ionization probability to be used in the binomial forms is obtained after integrating in the ejection electron space

$$\begin{aligned} p_{\rm nlm}(\vec{b}) &= \int dE \int d\Omega\, |a_{\rm nlm}(E,\Omega,\vec{b})|^2 \\ &= \frac{1}{2\pi} \sum_{\mu=-M}^{M} \int dE \int d\Omega\, |a_{{\rm nlm}\mu}(E,\Omega,b)|^2. \end{aligned} \quad (5)$$

The T-matrix elements were integrated numerically for different angular momenta and added appropriately. To be consistent, we consider $M = 2l_{\rm max} + 1$, where $l_{\rm max}$ is the maximum angular momentum used to solve the Schrödinger equation, which in our case ranged from $l_{\rm max} = 8$ to 28, depending on E. We followed the same procedure to calculate the T-matrix elements of previous papers [33]. Summarizing, for each state characterized by the quantum numbers n and l, a target central potential was determined from the Hartree-Fock wave functions. The initial (bound) and final (continuum) electron wave functions were expanded in spherical harmonics times radial wave functions obtained through the numerical solution of the radial Schrödinger equation.

As we are dealing with a dressed projectile, the projectile-electron interaction was calculated using the wave functions of $B^{2+}(1s^2 2s)$ given by Clementi and Roetti [28]. The resulting potential was fitted to

$$V_{B^{2+}}(r_P) = \frac{2}{r_P} + \sum_{j=1}^{2} \frac{Z_j}{r_P} e^{-\beta_1 r_P}, \quad (6)$$

where $Z_1 = 1.250$, $Z_2 = 1.750$, $\beta_1 = 1.376$, and $\beta_2 = 6.138$. To calculate the matrix element we rewrote the total Hamiltonian H of the system as

$$\begin{aligned} H &= H_{\rm atom} + K_{\rm proj} - V_{B^{2+}}(r_P) \\ &= H_{\rm atom} + K_{\rm proj} - \frac{Z_{\rm eff}(p)}{r_P} + \left[-V_{B^{2+}}(r_P) + \frac{Z_{\rm eff}(p)}{r_P} \right] \end{aligned}$$

where $H_{\rm atom}$ is the Hamiltonian of the target atom, $K_{\rm proj}$ is the kinetic energy operator of the projectile, and

$$Z_{\rm eff}(p) = \frac{p^2}{4\pi}\int d\vec{r}\; e^{i\,\vec{p}\,.\,\vec{r}}\; V_{B^{2+}}(r) \qquad (7)$$

$$= 2 + \sum_{j=1}^{2} \frac{Z_j\; p^2}{\left(\beta_j^2 + p^2\right)}. \qquad (8)$$

The strategy to tackle the problem was to calculate the CDW-EIS wave function of the kernel Hamiltonian $H_{\rm kernel} = H_{\rm atom} + K_{\rm proj} - Z_{\rm eff}(p)/r_P$ and its T-matrix element, considering $[-V_{B^{2+}}(r_P) + Z_{\rm eff}(p)/r_P]$ as a first perturbative order. Therefore the calculation resembles the one of a bare projectile with a Coulomb parameter $a_P = Z_{\rm eff}(p)/v_i$, where v_i is the ion velocity. The contribution of the residual potential given by the term in squared bracket is small, although larger than in the case of He^+ impact studied in [33].

The postcollisional contribution (Auger-like processes) was considered following Ref. [10], through the branching ratios $F_{nl,j}$ for recoil ions Ne^{j+} measured in photoionization experiments after single ionization of the nl subshell. The branching ratio values employed in this work for Ne were those by Landers [34], $F_{1s,1} = 0.0193$, $F_{1s,2} = 0.921$, $F_{1s,3} = 0.0571$, $F_{1s,4} = 0.0028$.

IV. RESULTS AND DISCUSSION

The measured cross section for multiple ionization of Ne by B^{2+} projectiles are displayed in Table I. Figure 1 shows the experimental results together with CDW-EIS calculations with (full lines) and without (dashed lines) postcollisional Auger-like transitions. This model is expected to be valid for energies above the theoretical maxima (i.e., 100 keV/amu for single ionization, higher energies for other final charge states of Ne). For lower impact energies, the CDW-EIS results fall down drastically.

The theoretical calculations for B^{2+} in Ne show rather good agreement with the experiments for the Ne^+ and Ne^{2+} recoil ions. On the other hand, for Ne^{3+} the CDW-EIS results are 50% above the data at 300 keV/amu, and they do not explain the Ne^{4+} and Ne^{5+} values. This tendency to overestimate the data for multiple ionization of Ne (final charge state $q \geqslant 3$) has already been observed [9,20] in different calculations within the independent particle model. It is an interesting point to study because similar calculations for other targets

TABLE I. Absolute single and multiple pure ionization cross sections (in Mb) of Ne by B^{2+} as a function of the projectile energy, E.

E (MeV)	Ne^+	Ne^{2+}	Ne^{3+}	Ne^{4+}	Ne^{5+}
0.75	268 ± 18	54 ± 4	20 ± 2	5.1 ± 0.6	
1.00	285 ± 20	64 ± 5	24 ± 2	8.1 ± 0.8	0.7 ± 0.2
1.50	281 ± 23	64 ± 5	26 ± 2	9.3 ± 1.0	1.0 ± 0.2
2.00	283 ± 29	64 ± 7	26 ± 3	11 ± 1.3	1.1 ± 0.2
2.50	291 ± 27	68 ± 7	25 ± 3	8.2 ± 1.0	1.2 ± 0.3
3.00	297 ± 27	66 ± 6	22 ± 2	7.6 ± 0.9	1.1 ± 0.3
3.50	317 ± 32	65 ± 7	23 ± 3	6.4 ± 0.9	0.8 ± 0.3
4.00	308 ± 32	62 ± 6	19 ± 2	5.2 ± 0.6	0.6 ± 0.1

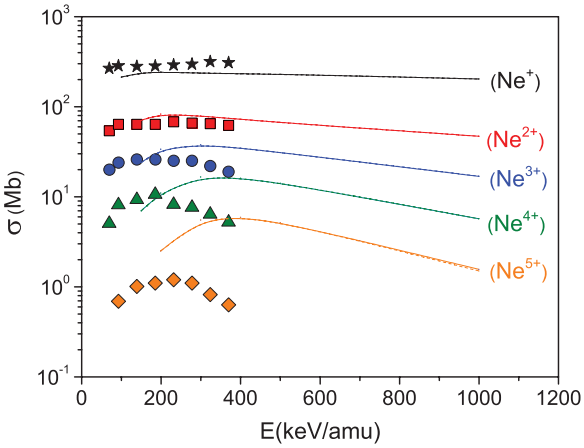

FIG. 1. (Color online) Cross sections for multiple ionization of Ne by B^{2+} as a function of the projectile energy. Experiment: stars, Ne^+; squares, Ne^{2+}; circles, Ne^{3+}; triangles, Ne^{4+}; lozenges, Ne^{5+}. Theory: full line, CDW-EIS with Auger; dashed lines, CDW-EIS without Auger. This last contribution is negligible.

probed to give good results [10]. A different physics appears in the case of Ne, which may be related to the importance of correlation among electrons, or to the influence of changes in the potential. In this sense Ne serves as a benchmark target for future research.

Although the postcollisional Auger decay was included, it is clear in Fig. 1 that this contribution is negligible for energies in the range of the present measurements. These calculations also show that the importance of postcollisional processes is shifted toward higher velocities for increasing projectile perturbing field when compared with the proton case. This fact was already noted by Tachino *et al.* [35] for molecular targets.

The relative Ne^{q+} recoil ion production due to pure ionization is shown in Fig. 2, where the ratios $\sigma(Ne^{q+})/\sum_1^5 \sigma(Ne^{q+})$are plotted. It can be seen from this figure that there is a good agreement between the experiment and the CDW-EIS calculations for small charge states and high

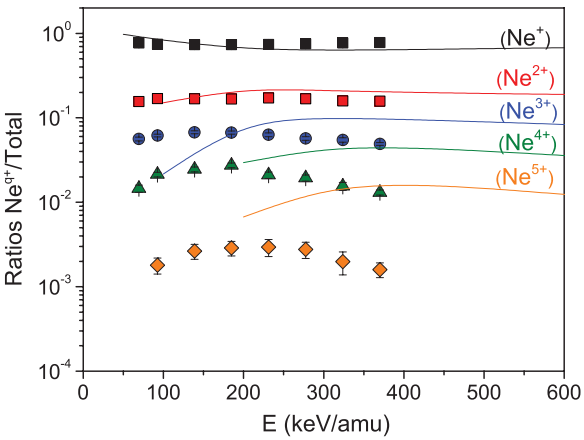

FIG. 2. (Color online) Cross section ratios for production of Ne^{q+} ions by pure ionization over the total ionization cross section. Closed symbols: experiment (as in Fig. 1). Full lines: CDW-EIS calculations.

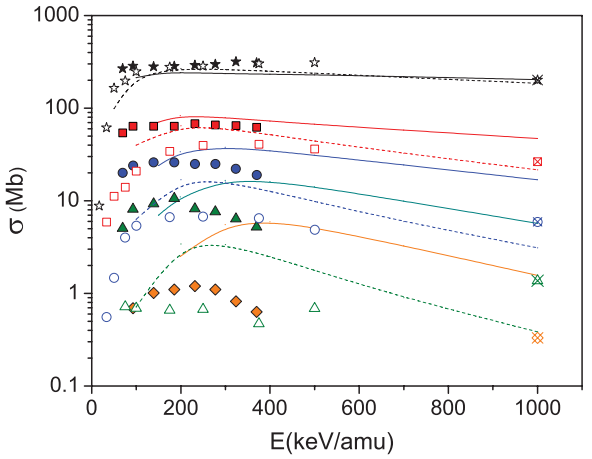

FIG. 3. (Color online) Cross sections for multiple ionization of Ne as a function of the projectile energy per amu. Experiment: stars, Ne^{+}; squares, Ne^{2+}; circles, Ne^{3+}; triangles, Ne^{4+}; lozenges, Ne^{5+}. Closed symbols B^{2+}, this work; open symbols He^{2+} (Ref. [37]); open crossed symbols F^{2+} (Ref. [24]). Theory: full line, CDW-EIS with Auger for B^{2+} projectiles (Ne^{+}up to Ne^{5+}); dashed lines, CDW-EIS with Auger for He^{2+} projectiles (Ne^{+} up to Ne^{4+}).

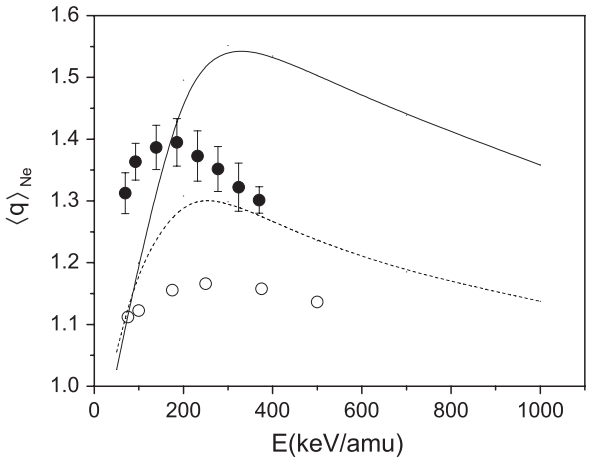

FIG. 4. Average charge state of the Ne recoil ions produced by pure ionization. Experiment: full circles, B^{2+} (this work); open circles, He^{2+} (Ref. [37]). Theory: CDW-EIS calculations: full curve, B^{2+}; dashed curve, He^{2+}.

velocities but, as the charge state increases, the calculations progressively overestimate these ratios for high velocities.

The average effective charge of the B^{2+} along the ionization path and the effectiveness of its electrons in shielding its nucleus can be studied by comparing the cross sections of multiple ionization of Ne by B^{2+} with bare He^{2+}. Figure 3 present results for B^{2+} (closed symbols as in Fig. 1), DuBois results for He^{2+} [37] (open symbols) and Heber *et al.* results for F^{2+} [24] (open crossed symbols). The full and dashed lines are CDW-EIS calculations for B^{2+} and He^{2+}, respectively, for the various charge states of the Ne recoils, $q = 1$–5 for B^{2+}, and $q = 1$–4 for He^{2+}.

The experimental data presented in this figure shows that dressed and bare projectiles—with the same charge state—produce recoil ion charge states with very different yields. This behavior is also described by the CDW-EIS calculations. For single ionization, B^{2+} and He^{2+} cross sections are quite similar. But the difference increases with the charge state of the Ne^{+q} recoil ion. For example, the cross sections for producing Ne^{4+} by B^{2+} are one order of magnitude larger than those obtained by He^{2+} projectiles at the same impact velocity. Dressed ions become more and more efficient in producing highly charged recoils as the collisions becomes closer and stronger.

Figure 4 displays the average recoil ion charge $\langle q\rangle_{\mathrm{Ne}}$ of the Ne recoil ions due to pure ionization by B^{2+} and He^{2+}, obtained by weighing the cross sections for q up to 4 in both cases

$$\langle q\rangle = \frac{\sum_1^4 q\sigma(\mathrm{Ne}^{q+})}{\sum_1^4 \sigma(\mathrm{Ne}^{q+})}. \tag{9}$$

The average recoil ion charge is larger for B^{2+} compared to He^{2+} projectiles for the reasons discussed above. This is an important result regarding the concept of the radiation damage in the region of the Bragg peak. Standard stopping power calculations scales with the projectile equilibrium charge state [36] assigning the same stopping power—and resulting damage—to different projectiles with the same equilibrium charge state and velocity. Present results show that this is not true. Moreover, the local damage is sensitive to the local charge left by the projectile in the track.

In the same line of reasoning, and to make a more global comparison, Fig. 5 displays the total cross section for ion production, $\sum_1^5 q\sigma(\mathrm{Ne}^{q+})$, due to the impact of B^{2+} and He^{2+} ions. The experiments, as well as the theory at large impact velocities (i.e., in the range of applicability of the present calculations) agree that the B^{2+} is a more efficient ionizer than the He^{2+} ion. The reason for that is the fact that the mean radius of B^{2+} $2s$ ion (0.87 Å) is larger than the Ne $2p$ one (0.52 Å) [28] and so quite ineffective in screening the projectile nucleus in close collisions, therefore increasing the net effective charge of B^{2+}. Alternatively, it can be clearly seen from Eq. (8) that at close collisions (hard collisions with p very

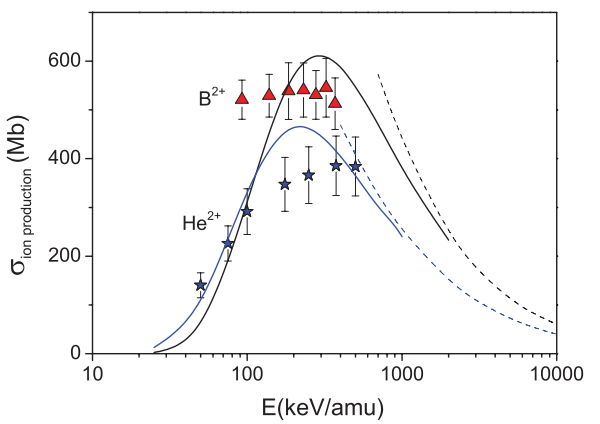

FIG. 5. (Color online) Cross section for positive ion production (see text) as a function of the impact energy per amu. Experiment: triangles, B^{2+} (this work); stars, He^{2+}(Ref. [37]). Theory: CDW-EIS calculations: full curves; Born approximation: dashed curves.

large) $Z_{\rm eff}(p) \to 2 + Z_1 + Z_2 = 5$, while at large distances (soft collisions with p very small) $Z_{\rm eff}(p) \to 2$.

A further evaluation of the role of the effective charge of the dressed B^{2+} projectile can be achieved by looking at the ratio of the cross sections with respect to the bare case. In order to obtain a meaningful scaling the independent particle model can be used. For simplicity let us consider the multiple ionization of the $2p$ shell of the neon target by a projectile charge Z. The exclusive ionization probabilities as a function of the impact parameter, b, can be written within the independent particle model as

$$\begin{aligned} P^{\rm Ne^{1+}}(b) &= p^1(b)[1-p(b)]^5 \\ P^{\rm Ne^{2+}}(b) &= p^2(b)[1-p(b)]^4 \\ &\cdots\cdots \\ P^{\rm Ne^{n+}}(b) &= p^n(b)[1-p(b)]^{6-n}. \end{aligned}$$

Considering that in the perturbative regime $p(b) \propto Z^2$ and $p(b) \ll 1$, then

$$\begin{aligned} P^{\rm Ne^{1+}}(Z,b) &= Z^2 P^{\rm Ne^{1+}}(Z=1,b) \\ P^{\rm Ne^{2+}}(Z,b) &= Z^4 P^{\rm Ne^{2+}}(Z=1,b) \\ &\cdots\cdots \\ P^{\rm Ne^{n+}}(Z,b) &= Z^{2n} P^{\rm Ne^{n+}}(Z=1,b), \end{aligned}$$

and the cross section for multiple ionization scales as:

$$\sigma^{\rm Ne^{n+}}(Z) = Z^{2n}\sigma^{\rm Ne^{n+}}(Z=1). \tag{10}$$

Therefore, we can define the effective charge Z_q, associated to Ne^{q+} ion production, as:

$$Z_q = \left[\frac{\sigma^{\rm Ne^{q+}}(Z)}{\sigma^{\rm Ne^{q+}}(Z=1)}\right]^{1/2q}, \tag{11}$$

or, taking the above equation with respect to He^{2+},

$$Z_q = 2\left[\frac{\sigma(B^{2+})}{\sigma(He^{2+})}\right]^{1/2q}. \tag{12}$$

If distant collisions dominate, Z_q should be equal to the projectile charge (2 in the present study). Figure 6 displays Z_q for each one of the Ne^{q+} final charge states, as a function of projectile energy. The experimental points are obtained, using the present measurements and those of DuBois [37] for He^{2+}, and the theoretical curves are the CDW-EIS results.

Experimental and theoretical results show an increase of the effective charge of B^{2+} with the ionization order $+q$, as already noted in Fig. 3. Although the experimental data show very different behavior as compared with the CDW-EIS results, they seem to converge to similar values for the higher energies measured. The increase of Z_q as the velocity decreases is an interesting feature of the experimental results that deserves further theoretical discussion. On the other hand, for large impact velocities, where Eq. (12) is valid, the theoretical curves show a clear incremental tendency. These results are expected considering that for higher energies inner-shell ionization plays an important role, which means close collisions.

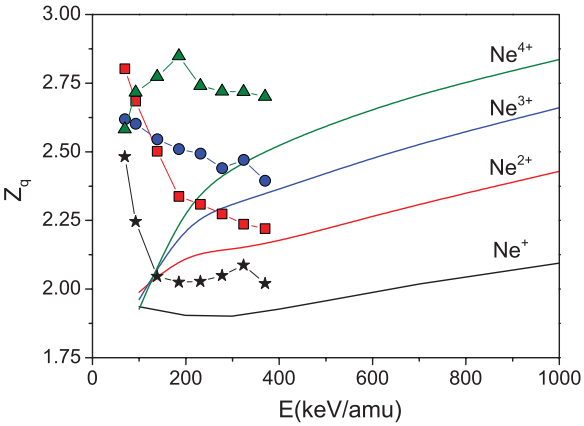

FIG. 6. (Color online) Effective charge, given by Eq. (12), of B^{2+} as a function of projectile velocity. Experiment: stars, Ne^{+}; squares, Ne^{2+}; circles, Ne^{3+}; triangles, Ne^{4+}. Theory: full lines, CDW-EIS.

V. CONCLUSION

We have measured exclusive cross sections for ionization of Ne colliding with B^{2+} projectiles, in the energy range from 0.75 to 4.0 MeV. Absolute cross section for production of Ne^{q+} recoils, with q up to 5 are reported. Calculations have been performed using the CDW-EIS model.

It was observed that the ionization cross sections by B^{2+}, mainly for the production of highly charged recoils, are strongly enhanced when compared to the bare projectile with the same charge state, He^{2+}, at the same velocities. This behavior was observed for all measured projectile energies, but it is particularly enhanced at lower velocities. CDW-EIS calculations confirmed that for close collisions the net charge state of the B^{2+} becomes larger than 2 because the nuclear screening by the B^{2+} electrons becomes less effective (weakened screening). This can be explained in terms of the inhomogeneous screening of the B^{2+} electrons, mainly the weak screening of the outer $2s$ electron. The use of the Hartree-Fock wave functions for the B^{2+} is shown to be very important to obtain an accurate description of the dressed projectile interaction.

The present CDW-EIS shows a good general agreement with the present experimental data for single and double ionization but overestimate the data for higher ionization orders. This is a general behavior of the independent particle model when dealing with Ne targets that deserves more research. On the other hand, more theoretical work is needed to describe the details of the enhancement of the ionization cross sections with respect to the bare projectile case.

The ionization of complex multielectron atoms and molecules by dressed projectiles, in the intermediate-velocity regime, has been poorly studied both experimentally and theoretically. This regime, which corresponds to the Bragg peak, where the stopping power of heavy projectiles in matter reaches its maximum value, is an important region of the projectile trajectory for many applications. Independently of

the projectile or the type of the material it goes through, when it reaches the Bragg peak region the projectile collects electrons (becomes dressed) due to the many charge-changing collisions that occur along its path. The understanding of the collision dynamics in this region is essential to obtain the local damage in the material. It was shown in this work that, although difficult to predict theoretically, the knowledge of how much the projectile screening has been weakened as it participates in the ionization process is a key point to predict such damage.

ACKNOWLEDGMENTS

This work was supported in part by the Brazilian agencies Conselho Nacional de Desenvolvimento Científico e Tecnológico (CNPq) and Fundação de Amparo à Pesquisa do Estado do Rio de Janeiro (FAPERJ) and by the Argentinian agencies Consejo Nacional de Investigaciones Cientificas y Técnicas (CONICET), the Agencia Nacional de Promoción Científica y Tecnológica (ANPCyT), and the University of Buenos Aires.

[1] J. H. McGuire and L. Weaver, Phys. Rev. A **16**, 41 (1977).
[2] H. J. Lüdde and R. Dreizler, J. Phys. B **18**, 107 (1985).
[3] J. H. McGuire, *Electron Correlation Dynamics in Atomic Collisions* (Cambridge University Press, Cambridge, 1997).
[4] M. M. SantAnna, E. C. Montenegro, and J. H. McGuire, Phys. Rev. A **58**, 2148 (1998).
[5] C. L. Cocke, Phys. Rev. A **20**, 749 (1979).
[6] R. E. Olson, J. Ullrich, and H. Schmidt-Bocking, J. Phys. B **20**, L809 (1987).
[7] R. E. Olson, J. Ullrich, and H. Schmidt-Bocking, Phys. Rev. A **39**, 5572 (1989).
[8] D. R. Schultz, R. E. Olson, C. O. Reinhold, S. Kelbch, C. Kelbch, H. Schmidt-Bocking, and J. Ullrich, J. Phys. B **23**, 3839 (1990).
[9] M. E. Galassi, R. D. Rivarola, and P. D. Fainstein, Phys. Rev. A **75**, 052708 (2007).
[10] C. C. Montanari, E. C. Montenegro, and J. E. Miraglia, J. Phys. B **43**, 165201 (2010).
[11] T. Kirchner, A. C. F. Santos, H. Luna, M. M. SantAnna, W. S. Melo, G. M. Sigaud, and E. C. Montenegro, Phys. Rev. A **72**, 012707 (2005).
[12] C. D. Archubi, C. C. Montanari, and J. E. Miraglia, J. Phys. B **40**, 943 (2007).
[13] E. G. Cavalcanti, G. M. Sigaud, E. C. Montenegro, M. M. SantAnna, and H. Schmidt-Bocking, J. Phys. B **35**, 3937 (2002).
[14] M. O. Krause, M. V. Vestal, W. H. Johnson, and T. A. Carlson, Phys. Rev. **133**, A385 (1964).
[15] T. A. Carlson and M. O. Krause, Phys. Rev. **137**, A1655 (1965).
[16] T. A. Carlson and M. O. Krause, Phys. Rev. **140**, A1057 (1965).
[17] T. A. Carlson and M. O. Krause, Phys. Rev. Lett. **14**, 390 (1965).
[18] M. O. Krause and T. A. Carlson, Phys. Rev. **149**, 52 (1966).
[19] T. A. Carlson, W. E. Hunt, and M. O. Krause, Phys. Rev. **151**, 41 (1966).
[20] T. Spranger and T. Kirchner, J. Phys. B **37**, 4159 (2004).
[21] G. Schenk and T. Kirchner, J. Phys. B **42**, 205202 (2009).
[22] T. J. Gray, C. L. Cocke, and E. Justiniano, Phys. Rev. A **22**, 849 (1980).
[23] T. Matsuo, T. Tonuma, H. Kumagai, and H. Tawara, Phys. Rev. A **50**, 1178 (1994).
[24] O. Heber, G. Sampoll, B. B. Bandong, R. J. Maurer, R. L. Watson, I. Ben-Itzhak, J. M. Sanders, J. L. Shinpaugh, and P. Richard, Phys. Rev. A **52**, 4578 (1995).
[25] J. Ullrich, K. Bethge, S. Kelbch, W. Schadt, H. Schmidt-Bocking, and K. E. Stiebing, J. Phys. B **19**, 437 (1986).
[26] Y. Sugizakit, M. Sataka, K. Kawatsura, T. Shirai, and Y. Nakai, J. Phys. B **22**, 263 (1989).
[27] A. C. F. Santos, W. S. Melo, M. M. SantAnna, G. M. Sigaud, and E. C. Montenegro, Phys. Rev. A **63**, 062717 (2001).
[28] E. Clementi and C. Roetti, At. Data and Nucl. Data Tables **14**, 177 (1974).
[29] M. M. SantAnna, H. Luna, A. C. F. Santos, C. McGrath, M. B. Shah, E. G. Cavalcanti, G. M. Sigaud, and E. C. Montenegro, Phys. Rev. A **68**, 042707 (2003).
[30] G. M. Sigaud, M. M. SantAnna, H. Luna, A. C. F. Santos, C. McGrath, M. B. Shah, E. G. Cavalcanti, and E. C. Montenegro, Phys. Rev. A **69**, 062718 (2004).
[31] H. Tawara and A. Russek, Rev. Mod. Phys. **45**, 178 (1973).
[32] W. Wolff, H. Luna, A. C. F. Santos, E. C. Montenegro, and G. M. Sigaud, Phys. Rev. A **80**, 032703 (2009).
[33] J. E. Miraglia and M. S. Gravielle, Phys. Rev. A **81**, 042709 (2010).
[34] A. L. Landers *et al.*, Phys. Rev. Lett. **102**, 223001 (2009).
[35] C. A. Tachino, M. E. Galassi, and R. D. Rivarola, Phys. Rev. A **80**, 014701 (2009).
[36] E. C. Montenegro, S. A. Cruz, and C. Vargas-Aburto, Phys. Lett. A **92**, 195 (1982).
[37] R. D. DuBois, Phys. Rev. A **36**, 2585 (1987).